Experimental determination of spin-transfer torque nonadiabaticity parameter and spin polarization in permalloy

S. Lepadatu,[1,*] M. C. Hickey,[1,†] A. Potenza,[2] H. Marchetto,[2,‡] T. R. Charlton,[3] S. Langridge,[3] S. S. Dhesi,[2] and C. H. Marrows[1,§]

[1]*School of Physics and Astronomy, E.C. Stoner Laboratory, University of Leeds, Leeds LS2 9JT, United Kingdom*

[2]*Diamond Light Source, Chilton, Didcot OX11 0DE, United Kingdom*

[3]*ISIS, STFC Rutherford Appleton Laboratory, Chilton, Didcot OX11 0QX, United Kingdom*

(Received 27 June 2008; revised manuscript received 8 December 2008; published 3 March 2009)

The domain-wall depinning boundary, showing the variation in critical current density with magnetic field, is measured for notched permalloy wires using pulsed-current measurements. The structure of domain walls trapped at the pinning potential provided by the notch is imaged using photoemission electron microscopy. The experimental depinning boundary is compared with those obtained by micromagnetic simulations including the adiabatic and nonadiabatic spin-torque terms. This method allows for the determination of both the nonadiabaticity parameter β and spin current polarization P, which we obtain as $\beta=0.040\pm0.005$ and $P=0.40\pm0.02$ at room temperature.

DOI: 10.1103/PhysRevB.79.094402 PACS number(s): 75.60.Ch, 72.25.Ba, 72.25.Pn

Current induced domain-wall movement[1] has been the focus of much recent research due to its promising device applications and interesting underlying physics. Theoretically, the interaction between spin-polarized currents and magnetization is described using additional spin-transfer torque terms added to the Landau-Lifshitz-Gilbert equation,[2,3]

$$\frac{\partial \mathbf{m}}{\partial t} = \gamma \mathbf{H}_{\text{eff}} \times \mathbf{m} + \alpha \mathbf{m} \times \frac{\partial \mathbf{m}}{\partial t} - u\frac{\partial \mathbf{m}}{\partial x} + \beta u \mathbf{m} \times \frac{\partial \mathbf{m}}{\partial x}, \tag{1}$$

valid for current applied along the x axis. Here $\boldsymbol{m}$ is the unit vector along the local magnetization direction, γ is the gyromagnetic ratio, α is the damping constant, and $u=JPg\mu_B/2eM_S$, where J is the charge current density, P is the spin current polarization, and M_S is the saturation magnetization. The last two terms on the right-hand side are the spin-transfer torque terms, namely, the adiabatic[4] and nonadiabatic spin-transfer torque.[2,3] The latter term was introduced to resolve discrepancies between experimental observations and theoretical predictions[4] and its contribution is determined by a dimensionless constant β known as the nonadiabaticity parameter, given by $\beta=\hbar/J_{\text{ex}}\tau_{\text{sf}}$,[3] where J_{ex} is the s-d exchange interaction energy and τ_{sf} is the spin-flip time. Although the current theoretical treatment is sufficient to explain the interaction between spin-polarized currents and domain walls, the exact value of β for various materials is still under debate. Zhang and Li[2] have argued that the value of β should be of the order of 10^{-2}, as confirmed by studies of current-driven domain-wall motion in permalloy nanowires.[5,6] A number of recent studies have investigated the value of β,[2,3,5–13] yielding a range of values. In a recent experiment,[12] the dynamics of domain-wall depinning was studied in permalloy wires by pulsed-current measurements and comparison of experimental results with micromagnetic modeling have yielded values of $\beta=0.016$ and $P=0.6$ for $\alpha=0.008$. Experimental observations of the current-induced domain-wall propagation in permalloy strips[3] were best reproduced for $\beta=0.04$ and $P=0.4$ for $\alpha=0.02$. On the other hand, the domain-wall depinning from a notch induced by a pulsed current[12] was reproduced for $\beta=0.016$ and $P=0.6$ for $\alpha=0.008$. The relationship between β and the damping constant α has also come under debate. Kohno *et al.*[14] have argued that generally $\beta\neq\alpha$, while other theoretical considerations have shown that β should equal α.[15–17] However, recent comparison of micromagnetic simulations with photoemission electron microscopy (PEEM) images of the spin structure transformations of domain walls in permalloy nanowires induced by current pulses[9] has shown that the observed domain-wall transformations may be reproduced only under the condition that $\beta\neq\alpha$. The determination of β is further complicated by uncertainties in the value of the spin polarization P, which was measured in the ballistic conduction regime using tunneling and superconducting point-contact experiments to be in the range 0.3–0.45 in permalloy[18–20] and diffusive conduction regime using current perpendicular to the plane (CPP) multilayers or ternary alloys[21–23] to be in the range 0.7–0.9. An entirely different approach was first proposed by Berger,[24] where the value of P in the bulk may be obtained by investigation of the interaction between spin-polarized currents and domain walls. This has been a long-standing problem and in view of recent theoretical advances it is now clear that experiments capable of simultaneously determining the values of both β and P are required.

In this work we use the method proposed by He *et al.*[25] to investigate the values of β and P in permalloy. Using a notched permalloy wire, the depinning boundary of a pinned domain wall, showing the variation of critical current density with magnetic field, is measured, and these results are compared with micromagnetic simulations including both the adiabatic and nonadiabatic spin-transfer torque terms. Since the action of the nonadiabatic spin-transfer torque is similar to that of a magnetic field, while the adiabatic torque is perpendicular to the nonadiabatic torque, for a fixed value of P the shape of the depinning boundary varies greatly with β. Thus by matching both the individual critical current values as well as the shape of the depinning boundary the values of β and P may be determined simultaneously.

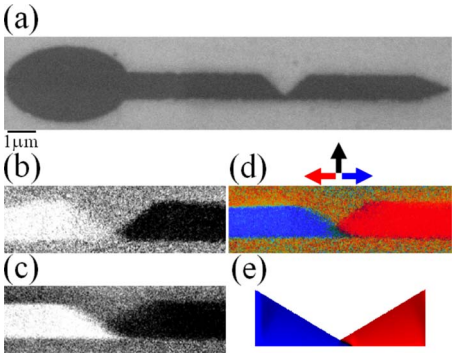

FIG. 1. (Color online) (a) SEM image of notched wire. [(b) and (c)] PEEM images of notched wire with 3 μm notch length showing a domain wall pinned at the notch. (d) in-plane PEEM vector map obtained from the two PEEM images in (b) and (c) taken with the x-ray beam at orthogonal angles. (e) Micromagnetic simulation of notched wire with 3 μm notch length showing a domain wall pinned at the notch.

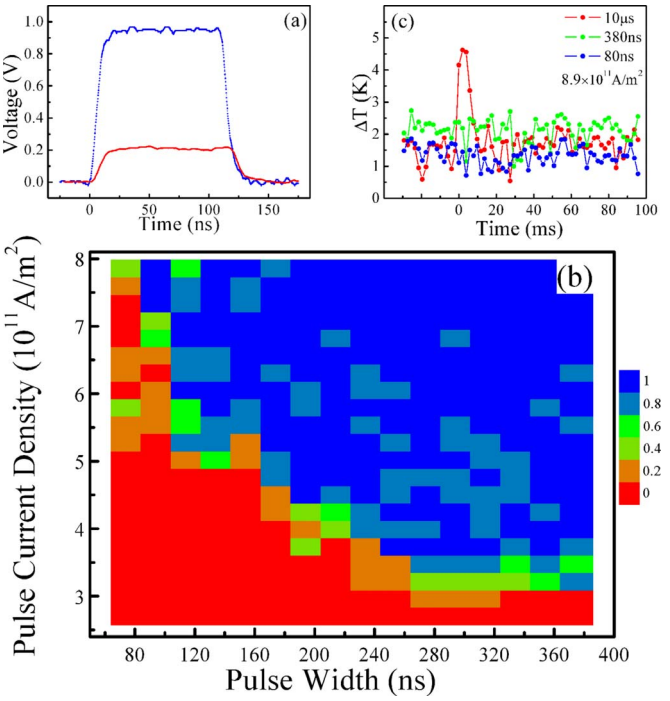

FIG. 2. (Color online) (a) Pulse from generator and resulting pulse across the sample. (b) Domain-wall depinning probability map, showing variation in critical current density as a function of pulse width for an applied longitudinal magnetic field of 14 Oe. (c) Temperature change in the sample as a result of Joule heating by current pulses of varying pulse width and fixed pulse amplitude resulting in a current density of 8.9×10^{11} A/m^2. The data points are acquired using an internal storage buffer on the lock-in amplifier.

Notched $Ni_{80}Fe_{20}$ wires of 20 nm thickness have been fabricated on Si/SiO_2 substrates using e-beam lithography, with the geometry shown by the scanning electron microscope (SEM) image in Fig. 1(a). The wire width is 1 μm, the constriction width 100 nm, and the notch length is 3 μm. An elliptical pad at one end is used to nucleate a domain wall after reversal from saturation. The process of domain-wall pinning at the notch consists of first saturating the wire with a large longitudinal magnetic field (i.e., along the axis of the wire), of magnitude greater than 500 Oe in all the transport measurements we shall report below, following which a reverse field of 10 Oe is applied. The application of a 10 Oe reverse field first switches the magnetization direction in the elliptical pad while maintaining the magnetization direction in the wire, owing to the different coercivities of the ellipse and wire, following which the domain wall nucleated in the ellipse is moved along the wire by the applied magnetic field and pinned at the notch. The magnetization switching mechanism and structure of the domain wall pinned at the notch was investigated by means of x-ray magnetic circular dichroism PEEM imaging with the I06 beamline at the Diamond Light Source synchrotron. Imaging was carried out at nominally zero field (less than 1 Oe), after saturation in 700 Oe and the application of a 10 Oe reverse field to nucleate and propagate the wall to the notch. Circularly polarized x-ray photons with energies corresponding to the Fe L_3 and L_2 absorption edges have been used. In order to obtain the structure of the pinned domain wall two PEEM images of the wire are taken with orthogonal angles of the x-ray beam with respect to the wire axis, as shown in Figs. 1(b) and 1(c), where the x-ray beam makes an angle of $\pm45°$ to the wire in both cases. These images represent the projection of the magnetization along the direction of the x-ray beam in the two orthogonal directions, respectively, encoded in gray-scale. By combining these two images using the standard blue-black-red color coding, the in-plane magnetization vector map is obtained as shown in Fig. 1(d). The structure of the pinned domain wall is also investigated by micromagnetic simulations using the object-oriented micromagnetic framework (OOMMF) package[26] with parameters characteristic of $Ni_{80}Fe_{20}$ and damping constant α of 0.02.[27] A vortex domain wall is introduced in the left-hand side of the notch and the system is left to relax in a 10 Oe longitudinal magnetic field. After the system achieves a stable state (stopping condition of $|M\times H|/Ms^2<10^{-5}$), the magnetic field is set to zero and the final state is obtained as shown in Fig. 1(e). A good agreement between the PEEM vector map and simulation result is obtained, showing a domain wall pinned near the center of the notch.

The depinning behavior of the domain wall under the influence of a spin-polarized current is investigated using pulsed-current measurements at room temperature. Pulsed-current measurements allow for much larger current-density values to be applied, compared to dc measurements, due to the much reduced time-averaged Joule heating of the wires. The voltage transmission coefficient, defined as the pulse voltage amplitude across the sample divided by the pulse voltage amplitude from the pulse generator, is measured to be around 0.21 as shown in Fig. 2(a), where both the initial and transmitted pulses are shown for an initial pulse of 1 V amplitude, 100 ns width, and 20 ns rise time. The transmitted voltage pulse is measured across the contact pads on the sample. Since the contact pads have a small resistance (less than 1 Ω) and have a small separation (less than 2 mm), then no further reflections are expected to arise from the

contact pads, and the measured transmitted voltage pulse is effectively the voltage pulse across the $Ni_{80}Fe_{20}$ wire. Using the measured value of the transmission coefficient and sample resistance (around 820 Ω), the amplitudes of the voltage pulses used in the measurements are converted into current-density values corresponding to the cross-sectional area at the constriction.

The dependence of the critical current density on pulse width and applied longitudinal magnetic field was investigated using the following procedure: (i) a domain wall was pinned at the constriction using a 10 Oe reversal field and detected by measuring the sample resistance. When a domain wall is pinned at the notch, its associated anisotropic magnetoresistance (AMR) contribution causes the wire resistance to decrease,[28] allowing the presence of a domain wall to be detected. (ii) The measurement field was set, and a single voltage pulse of given amplitude and duration was applied to the sample. The pulse polarity was selected so that the resulting spin-transfer torque acts in the same direction as the magnetic field electrons flowing from left to right in Fig. 1(a). (iii) The depinning of the domain wall was tested for by increasing the magnetic field past the depinning field value and measuring any resulting resistance change. By increasing the applied longitudinal magnetic field, a domain wall present at the constriction is removed at a field known as the depinning field, which in this case was measured to be around 15 Oe. Following the application of the voltage pulse, if the domain wall was depinned then no change in resistance was measured, while if the domain wall was not depinned an increase in resistance was registered at the depinning field value due to the AMR associated with the domain wall. For each combination of pulse amplitude and pulse width this procedure was repeated six times and the depinning probability obtained. For an applied magnetic field of 14 Oe the resulting depinning probability map is shown in Fig. 2(b). Here the depinning probability is shown using a color map ranging from red (zero probability) to blue (probability of 1), as a function of current density and pulse width. A depinning boundary is formed by the dependence of the critical current density on the pulse width marked by a transition region from the region of no depinning (red) to the region of depinning (blue). To obtain the exact dependence of the mean critical density on pulse width, the following method was used. For each fixed pulse width, we assumed that the probability distribution of domain-wall depinning as a function of current density could be fitted using the cumulative Gaussian distribution function, $\Phi=\{1+\mathrm{erf}[(J-\mu)/\sigma\sqrt{2}]\}/2$, where J is the current density and μ and σ are the fitting parameters, namely, the mean critical current density and standard deviation, respectively. The same procedure was repeated for the applied longitudinal magnetic field values down to 0 Oe to obtain the depinning boundaries and the results are shown in Fig. 3. The standard deviation was found to be $\sim 10^{10}$ A/m^2 in all cases.

The dependence of the critical current density on magnetic field is addressed in the next paragraph, but first the dependence on pulse width is discussed. One possible cause for the observed dependence of the critical current density on pulse width might be due to the increased Joule heating of the wire with increasing pulse width. It is known that Joule heating results in increased sample resistance and decreased critical current values.[29] Because of the dependence of sample temperature on sample resistance we can quantify the relative contribution of this effect for the different pulse width values used in the measurements. The resistance of the sample was continuously measured using a lock-in amplifier (sampling frequency of 512 Hz) with the time constant set to 1 ms, as a pulse of fixed amplitude is applied to the sample, for different pulse width values. The results for three different pulse width values, namely, 80 ns, 380 ns, and 10 μs, are shown in Fig. 2(c), where the current density used was 8.9×10^{11} A/m^2. For the 10 μs pulse width a jump in the resistance value is observed as the pulse is applied, indicating a rapid increase in the sample temperature of ~4 K, following which the resistance decreases to its initial value due to the decaying temperature of the sample. The resistance change is converted to temperature change by assuming a linear dependence using the gradient measured in similar NiFe wires.[29] On the other hand for the 80 and 380 ns pulse width this effect is not observed. Therefore the heating of the sample by the applied pulses cannot explain the dependence of the critical current density on pulse width shown in Fig. 2(b). With each domain-wall depinning event there is an associated depinning time. Thus if the pulse width is sufficiently reduced, that is, if the spin-transfer torque acting on the domain wall is stopped before the domain wall has cleared the pinning potential, then depinning will no longer occur as the domain wall returns to its starting position under the action of the pinning potential. To compensate for the reduced pulse width the current density must then be increased so as to reduce the depinning time. On the other hand, if the pulse width is longer than the depinning time then further increasing the pulse width will not result in lower critical current-density values, assuming the Joule heating is not significantly increased. This latter effect is observed in the depinning boundaries shown in Fig. 3, where the critical current density approaches a limiting value as the pulse width is increased. The depinning time is also calculated using micromagnetic simulations, as detailed below, showing values of the order of 100 ns. Thus the largest pulse width value used, namely, 380 ns, was larger than the depinning time in all cases while still resulting in negligible Joule heating.

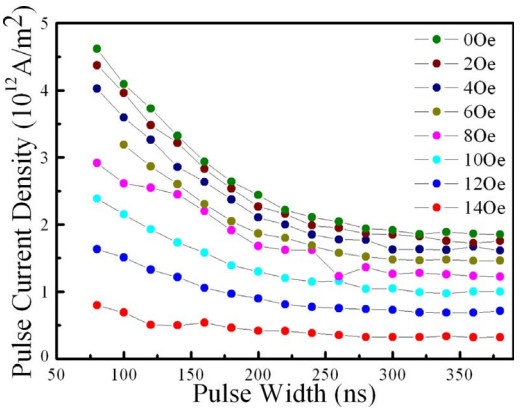

FIG. 3. (Color online) Domain-wall depinning boundary as a function of pulse width for different magnetic field values.

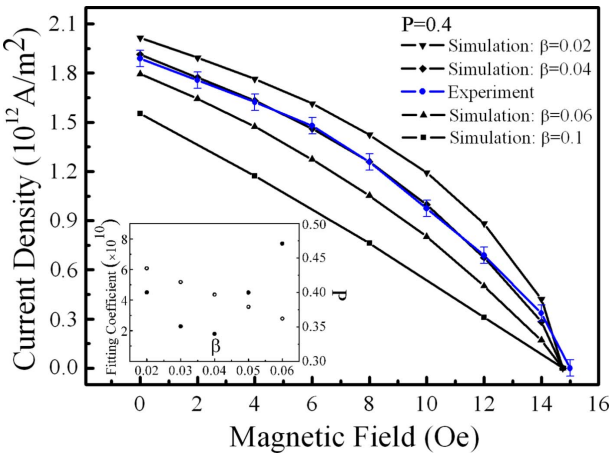

FIG. 4. (Color online) Experimental domain-wall depinning boundary, together with associated error bars, as a function of magnetic field for fixed pulse width of 380 ns, and simulated depinning boundaries for different values of nonadiabaticity parameter and spin polarization 0.4. In the inset, the fitting coefficient (solid circles) and best fit spin polarization (open circles) are plotted as a function of nonadiabaticity parameter.

Returning to the dependence of the critical current density on applied magnetic field, for the fixed pulse width of 380 ns, using the data shown in Fig. 3, the depinning boundary is plotted as a function of magnetic field in Fig. 4. In order to reproduce the measured depinning boundary, a modified version of the OOMMF software was used,[30] where the Landau-Lifshitz-Gilbert equation is modified by including the adiabatic and nonadiabatic spin-transfer torque terms as shown in Eq. (1).[2,3] Equation (1) is valid in the case where the current is aligned with the wire axis, taken as the x direction. As above, parameters typical of $Ni_{80}Fe_{20}$ at room temperature were used. The nonadiabaticity parameter β was varied in steps of 0.01 and for each fixed value of β the theoretical depinning boundary was calculated. The starting state used is shown in Fig. 1(e), as discussed above, and for each fixed magnetic field value the critical value of u was determined, where, in permalloy, the current density J is related to u by the formula $u=JP\times 7.24\times 10^{-11}$. This was done by running a set of simulations with different values of u and noting the final state (either domain wall is depinned in the final state or not) to determine the critical value of u. This allows for the variation of u with H to be obtained for the different values of β. Following this, the variation of J with H is plotted by setting the value of P to give the best fit to the experimental depinning boundary. The results for $\beta=0.1$, 0.06, 0.04, and 0.02 are shown in Fig. 4, where the damping parameter α was set to 0.02.[27] Here for the calculated boundary with $\beta=0.04$, the best fit to the experimental boundary was obtained for $P=0.4$. As expected, both the shapes of the depinning boundaries as well as the critical current-density values vary with β. Thus, for each fixed value of β, P was varied to obtain the best fit to the experimental boundary and a fitting coefficient was calculated. Here the fitting coefficient is defined as the average distance on the y axis between the points of the simulated and experimental boundaries, and the value of P is calculated so as to minimize the fitting coefficient.

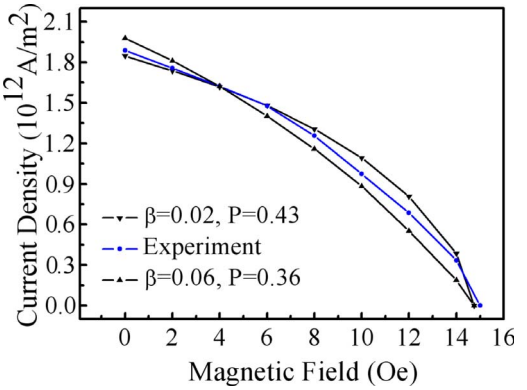

FIG. 5. (Color online) Experimental domain-wall depinning boundary and calculated boundaries for $\beta=0.02$ and 0.06 showing the best fit for P.

The resulting minimized fitting coefficients for the different values of β used in the simulations are shown on the inset of Fig. 4, and we obtain the best fit for $\beta=0.040$ (± 0.005) with the corresponding $P=0.40$ (± 0.02). As a comparison, the best fits obtained for $\beta=0.02$ and 0.06 are plotted in Fig. 5, showing the shape mismatch between the experimental and calculated depinning boundaries. The error margin for the nonadiabaticity parameter arises since β is varied in steps of 0.01. The error margin for current spin polarization arises due to experimental error margins. The value of P was determined to three decimal places as 0.397 from the fitting procedure, thus we obtain $P=0.40\pm 0.02$.

To investigate the dependence of β and P on the damping parameter α, the above fitting procedure was repeated using the lower value $\alpha=0.01$ obtained in 20 nm thick $Ni_{80}Fe_{20}$ thin films.[31] The fitting procedure results in a minimum value of the fitting coefficient for the pair of values $\beta=0.04$ (± 0.005) and $P=0.41$ (± 0.02). Comparison with the values of β and P obtained for $\alpha=0.02$ shows that the nonadiabaticity parameter is not changed within the experimental error for the lower value of α. Since β and P are obtained from micromagnetic modeling of the depinning behavior of a pinned domain wall, this indicates that the lower value of α does not influence the threshold currents significantly. The values of β and P obtained here are in rather good agreement with those obtained in current-driven domain-wall motion in permalloy strips[3] where the value of $\alpha=0.02$ was used. Comparison of theoretical work[13] with experiments[32] on the resonant depinning of a domain wall from a notch, where the values of $\alpha=0.02$ and $P=0.7$ were used, the nonadiabatic parameter was deduced as $\beta=0.04$. However, in a related domain-wall depinning experiment on notched permalloy wires[12] the values of β and P were obtained as 0.016 and 0.6 for a damping constant $\alpha=0.008$. The different values of β might be due to the different current spin-polarization values or possibly different material growth methods. Our results suggest that the value of the nonadiabaticity parameter is not changed by the value of the damping constant, however further experiments are required to understand the relationship between α, β, and P.

When comparing the simulations and experimental results, the main difference is the exclusion of thermal activa-

tion effects in the OOMMF simulation code. Thermal activation effects result in finite probability of jumping out of the pinning potential and this effect increases with temperature.[33–35] This can lead to the depinning boundary no longer being abrupt (as it is at 0 K), consistent with what is seen in Fig. 2(b) where the transition between the depinning and no depinning regimes occurs gradually. The probability of domain-wall depinning after a time t is given by $P(t)=\exp(-t/\tau)$ with $\tau=\tau_0\exp(E/k_BT)$, where τ_0 is the inverse of the attempt frequency and E is the energy barrier.[29] For small pinning potentials this can lead to a reduction in the critical current-density values and depinning fields with increasing temperature, as confirmed in a previous study on NiFe ring structures for a domain wall pinned at a defect in the wire.[7] On the other hand this effect is expected to be negligible for the case of large pinning potentials. Thus for the calculated depinning boundaries shown in Fig. 4, for a combination of current density and magnetic field below the depinning boundary, we find that the domain wall is displaced away from the starting position before settling to the final position within the notch structure. As the domain wall is displaced, the energy of the system increases and we denote by E_D the largest value of energy thus obtained. The overall energy barrier, E_P, is found to be around 10^{-13} J (that is 10^{-13} J must be used to completely remove the domain wall from its initial starting position) and for each combination of current density and magnetic field below the depinning boundary we obtain the effective energy barrier as $E=E_P-E_D$. Using the values obtained from micromagnetic simulations we find that typically for a reduction of 5×10^{10} A/m^2 (i.e., $\sim5\%$) in current density below the critical current density, the effective energy barrier E is of the order of 10^{-15} J. Since at room temperature $E=10^{-15}$ J is several orders of magnitude greater than k_BT, this results in vanishing probability of domain-wall depinning. Thus we may conclude that any reduction in the critical current-density values at room temperature, compared to 0 K, is negligible (i.e., within the experimental error). This is corroborated by noting that the measured depinning field value, for zero current density, is close to the calculated value. The experimental fact that the depinning is stochastic near to the phase boundary could also be connected with the fact that the pinning potential differs slightly for different wall structures and chiralities.[36]

In conclusion, using pulsed-current measurements we have investigated the dependence of domain-wall depinning, in a notched wire, on pulse amplitude, pulse width, and magnetic field. The structure of a domain wall trapped in the pinning potential was investigated using PEEM imaging. The depinning boundary, showing the dependence of the critical current density on magnetic field, was measured and this was compared with micromagnetic simulations including both the adiabatic and nonadiabatic spin-transfer torque contributions. By varying the value of the nonadiabaticity parameter β, we find $\beta=0.040\pm0.005$ and $P=0.40\pm0.02$ at room temperature.

This research was supported by the ESF EUROCORES collaborative research project SpinCurrent under the Fundamentals of Nanoelectronics program, and by the EPSRC through the Spin@RT consortium. We are grateful to the Diamond Light Source for the provision of beamtime. We would like to thank A. Vanhaverbeke for sharing the OOMMF extension code with us prior to public release and L. Bogart for assistance with the PEEM imaging.

*s.lepadatu@leeds.ac.uk
†Present address: Francis Bitter Magnet Laboratory, Massachusetts Institute of Technology, 150 Albany Street, Cambridge, Massachusetts 02139, USA.
‡Present address: Fritz Haber Institute, Faradayweg 4-6, 14195 Berlin, Germany.
§c.h.marrows@leeds.ac.uk

[1] C. H. Marrows, Adv. Phys. **54**, 585 (2005).
[2] S. Zhang and Z. Li, Phys. Rev. Lett. **93**, 127204 (2004).
[3] A. Thiaville, Y. Nakatani, J. Miltat, and Y. Suzuki, Europhys. Lett. **69**, 990 (2005).
[4] Z. Li and S. Zhang, Phys. Rev. B **70**, 024417 (2004).
[5] M. Hayashi, L. Thomas, Y. B. Bazaliy, C. Rettner, R. Moriya, X. Jiang, and S. S. P. Parkin, Phys. Rev. Lett. **96**, 197207 (2006).
[6] G. S. D. Beach, C. Knutson, C. Nistor, M. Tsoi, and J. L. Erskine, Phys. Rev. Lett. **97**, 057203 (2006).
[7] P. Dagras, M. Kläui, M. Laufenberg, D. Bedau, L. Vila, G. Faini, C. A. F. Vaz, J. A. C. Bland, and U. Rüdiger, J. Phys. D **40**, 1247 (2007).
[8] M. Laufenberg, W. Bührer, D. Bedau, P.-E. Melchy, M. Kläui, L. Vila, G. Faini, C. A. F. Vaz, J. A. C. Bland, and U. Rüdiger, Phys. Rev. Lett. **97**, 046602 (2006).
[9] L. Heyne, M. Kläui, D. Backes, T. A. Moore, S. Krzyk, U. Rüdiger, L. J. Heyderman, A. F. Rodriguez, F. Nolting, T. O. Mentes, M. Á. Niño, A. Locatelli, K. Kirsch, and R. Mattheis, Phys. Rev. Lett. **100**, 066603 (2008).
[10] E. Martinez, L. Lopez-Diaz, O. Alejos, L. Torres, and C. Tristan, Phys. Rev. Lett. **98**, 267202 (2007).
[11] M. Hayashi, L. Thomas, C. Rettner, R. Moriya, Y. B. Bazaliy, and S. S. P. Parkin, Phys. Rev. Lett. **98**, 037204 (2007).
[12] M. Hayashi, L. Thomas, C. Rettner, R. Moriya, and S. S. P. Parkin, Appl. Phys. Lett. **92**, 162503 (2008).
[13] E. Martinez, L. Lopez-Diaz, O. Alejos, and L. Torres, Phys. Rev. B **77**, 144417 (2008).
[14] H. Kohno, G. Tatara, and J. Shibata, J. Phys. Soc. Jpn. **75**, 113706 (2006).
[15] Y. Tserkovnyak, H. J. Skadsem, A. Brataas, and G. E. W. Bauer, Phys. Rev. B **74**, 144405 (2006).
[16] M. D. Stiles, W. M. Saslow, M. J. Donahue, and A. Zangwill, Phys. Rev. B **75**, 214423 (2007).
[17] S. E. Barnes and S. Maekawa, Phys. Rev. Lett. **95**, 107204 (2005).
[18] R. J. Soulen, Jr., J. M. Byers, M. S. Osofsky, B. Nadgorny, T. Ambrose, S. F. Cheng, P. R. Broussard, C. T. Tanaka, J. Nowak, J. S. Moodera, A. Barry, and J. M. D. Coey, Science **282**, 85 (1998).

[19] R. Meservey and P. M. Tedrow, Phys. Rep. **238**, 173 (1994).
[20] J. S. Moodera, J. Nowak, and R. J. M. van de Veerdonk, Phys. Rev. Lett. **80**, 2941 (1998).
[21] J. Bass and W. P. Pratt, Jr., J. Magn. Magn. Mater. **200**, 274 (1999).
[22] I. A. Campbell and A. Fert, in *Ferromagnetic Materials*, edited by E. P. Wohlfarth (North-Holland, Amsterdam, 1982), Vol. 3, Chap. 9.
[23] J. W. F. Dorleijn, Philips Res. Rep. **31**, 287 (1976).
[24] L. Berger, J. Appl. Phys. **49**, 2156 (1978).
[25] J. He, Z. Li, and S. Zhang, J. Appl. Phys. **98**, 016108 (2005).
[26] M. J. Donahue and D. G. Porter, Interagency Report NISTIR No. 6376, 1999 (unpublished); http://math.nist.gov/oommf.
[27] Y. Nakatani, A. Thiaville, and J. Miltat, Nature Mater. **2**, 521 (2003).
[28] K. Miyake, K. Shigeto, K. Mibu, T. Shinjo, and T. Ono, J. Appl. Phys. **91**, 3468 (2002).
[29] A. Yamaguchi, S. Nasu, H. Tanigawa, T. Ono, K. Miyake, K. Mibu, and T. Shinjo, Appl. Phys. Lett. **86**, 012511 (2005).
[30] A. Vanhaverbeke, http://www.zurich.ibm.com/st/magnetism/spintevolve.html.
[31] J. O. Rantschler, B. B. Maranville, J. J. Mallett, P. Chen, R. D. McMichael and W. F. Egelhoff, Jr., IEEE Trans. Magn. **41**, 3523 (2005).
[32] D. Bedau, M. Kläui, S. Krzyk, U. Rüdiger, G. Faini, and L. Vila, Phys. Rev. Lett. **99**, 146601 (2007).
[33] L. Néel, Ann. Geophys. (C.N.R.S.) **5**, 99 (1949); W. F. Brown, Phys. Rev. **130**, 1677 (1963).
[34] D. Atkinson, D. A. Allwood, G. Xiong, M. D. Cooke, C. C. Faulkner, and R. P. Cowburn, Nature Mater. **2**, 85 (2003).
[35] D. Atkinson, D. A. Allwood, C. C. Faulkner, G. Xiong, M. D. Cooke, and R. P. Cowburn, IEEE Trans. Magn. **39**, 2663 (2003).
[36] M. Hayashi, L. Thomas, C. Rettner, R. Moriya, X. Jiang, and S. S. P. Parkin, Phys. Rev. Lett. **97**, 207205 (2006).